JOURNAL OF GUIDANCE, CONTROL, AND DYNAMICS
Vol. 24, No. 2, March–April 2001

Reusable Launch Vehicle Control Using Linear-Adaptive and Subspace-Stabilization Techniques

C. Tournes*
Davidson Enterprises, LLC, Huntsville, Alabama 35806
and
C. D. Johnson†
University of Alabama in Huntsville, Huntsville, Alabama 35899

New robust flight control laws are developed for a reusable launch vehicle. The wide range of flight conditions, and the impossibility to obtain wind-tunnel data for most of the flight domain, requires using a robust control technique. The use of linear-adaptive control techniques to design the trajectory autopilot and to solve the inversion problem is proposed. Subspace-stabilization techniques are used to design the inner loop of control, which controls the vehicle attitude. The control is structured in two layers. The outer layer plays the role of an automatic pilot offering two operational modes: a trajectory mode and an attitude mode. In the trajectory mode the flight path and ground track are controlled, and in the attitude mode the autopilot controls attitude angles. The commands generated by the automatic pilot are inverted, by the use of a new and rather novel algorithm, to determine the required pitching, rolling, and yawing rate commands, which are then tracked by the inner loop of control. The inversion implements either bank-to-turn or skid-to-turn steering. The linear-adaptive methodology circumvents the use of difficult nonlinear control techniques and attendant analysis uncertainties through the use of linear disturbance accommodation observers to estimate and cancel the combined effects of nonlinear and/or uncertain terms. Subspace-stabilization techniques are used to steer the system error state to a certain subspace S representing the described or specified servotracking error behavior, while controlling the motion on the subspace S to the origin in error space. Some numerical simulation results are presented to demonstrate that the closed-loop response, with the proposed flight-control law, accurately tracks the prescribed flight and ground track trajectories.

Introduction

MULTIPLE-INPUT/MULTIPLE-OUTPUT aircraft and reusable launch vehicle (RLV) control problems have received considerable attention in recent years. Conventional single-input/single-output control design techniques have been used in the design of first generation fly-by-wire combat aircraft and several transport aircraft. Those designs are based on piecewise linearization of the plant and on a scheduling of control gains. Feedback linearization[1–4] addresses the nonlinear nature of the problem. The combined use of feedback linearization with linear H_∞ design has been investigated[5,6] where the H_∞ controller is used to improve the robustness to model uncertainties.

Tournes and Shtessel[7] and Tournes[8] have investigated the application of sliding mode control as a means of achieving both stability and performance robustness. A discontinuous bang–bang-type control is used to move the system's state to the sliding surface and rapid switching (chattering) of that control is used to keep it on the surface thereafter. The smoothed sliding mode control[9] approach consists of replacing the discontinuous relay control by an ad hoc linear saturation control law that is valid within a boundary layer of the sliding surface.

Flight Control Problems

The inversion problem in flight control consists of calculating the required inner-loop pitching, rolling, and yawing rate commands from the multiple commands generated by an outer-loop autopilot that controls the flight-path angle γ and the ground track angle χ. Those commands must to be transformed into commanded angle of attack α, sideslip angle β, and bank angle ϕ and then into pitch, roll, and yaw rates q, p, and r. To accomplish the required inversion, Bugasjski and Enns[10] propose using a matrix formulation and the use of pseudoinverses. References 4–6 and 11 also propose using feedback linearization techniques. Tournes and Shtessel[7] and Tournes[8] introduce the required nullity of the sideslip angle as an additional relation, as well as special filters that enforce desired flying qualities to provide the derivatives required for inverting the dynamics.

Tournes and Johnson[12–14] have proposed an alternative technique that tracks trajectory angles in the outer loop and calculates prescribed pitching, yawing, and rolling rates to be tracked in the inner loop, which achieves outer-loop commanded accelerations and a zero value of the sideslip angle. An innovative linear-adaptive controller is then used to compensate for small inversion errors appearing in the inversion of angle of attack, sideslip angle, and bank angle. Such errors are caused by model uncertainties relating the desired acceleration of the angle of attack and bank angle.

The proposed novel method for accomplishing inversion, applicable to both aircraft and to turn-to-bank RLV, uses on-line estimation of residual uncertainties in the inversion model. Those residuals are estimated in real time using disturbance observer[15–18] techniques and are used to effectively compensate for residuals in the calculations of the inversion.

The dynamics of the flight-path angle and of the ground track angle can be described by the set of first-order differential equations (1) and (2). With reference to Fig. 1 for the corresponding forces and moments, the two equations, describing the dynamics of the trajectory in velocity axes, are[6]

$$\dot{\gamma} = \frac{\cos\phi}{m\,\mathrm{vel}}F_Z - \frac{\sin\phi\cos\beta}{m\,\mathrm{vel}}F_Y - \frac{\cos\gamma}{\mathrm{vel}}g + \frac{T_Z\cos\phi}{m\,\mathrm{vel}} + \frac{T_Y\sin\phi\cos\beta}{m\,\mathrm{vel}} \tag{1}$$

$$\dot{\chi} = \frac{\sin\phi}{\cos\gamma\, m\,\mathrm{vel}}F_Z + \frac{\cos\phi\cos\beta}{\cos\gamma\, m\,\mathrm{vel}}F_Y + \frac{\sin\phi}{\cos\gamma\, m\,\mathrm{vel}}T_Z + \frac{\cos\phi\cos\beta}{\cos\gamma\, m\,\mathrm{vel}}T_Y \tag{2}$$

Presented as Paper 98-4119 at the AIAA Guidance, Navigation, and Control Conference, Boston, MA, 10–12 August 1998; received 5 April 1999; revision received 17 February 2000; accepted for publication 5 May 2000.

*Chief Scientist. Senior Member AIAA.
†Professor, Department of Electrical and Computer Engineering.

where the variables γ, χ, and ϕ represent, respectively, flight-path, ground track, and bank angles, and F_Z, F_Y, T_Z, and T_Y represent lift force, side force, and the normal and transverse thrust. The aircraft trajectory is determined by the combined effects of F_Z, F_Y, T_Z, and T_Y; moreover, assuming that the additional condition $\beta \approx 0$, leading to $F_Y + T_Y \approx 0$, is imposed, the flight-path trajectory is governed by $(F_Z + T_Z)\cos\phi$, and the ground track is governed by $(F_Z + T_Z)\sin\phi$. Thus, Eqs. (1) and (2) can be written as

$$\dot{\gamma} = \frac{\cos\phi(F_Z + T_Z)}{m\ \text{vel}} - \frac{g\cos\gamma}{\text{vel}} \tag{3}$$

$$\dot{\chi} = \frac{\sin\phi(F_Z + T_Z)}{m\ \text{vel}\cos\gamma} \tag{4}$$

We will represent the prescribed flight path and ground track angles by $\gamma^*(t)$ and $\chi^*(t)$, respectively, where the time dependency is sometimes omitted to simplify notation. Thus, Eqs. (3) and (4) can be represented in errors as

$$\dot{e}_\gamma = \dot{\gamma}^* - \frac{\cos\phi(F_Z + T_Z)}{m\ \text{vel}} + \frac{g\cos\gamma}{\text{vel}} \tag{5}$$

$$\dot{e}_\chi = \dot{\chi}^* - \frac{\sin\phi}{m\ \text{vel}\cos\gamma}(F_Z + T_Z) \tag{6}$$

where $e_\gamma = \gamma^* - \gamma$ and $e_\chi = \chi^* - \chi$. The total lift is represented as the following sum of the contributions of the angle of attack α, the deflection of pitch aerodynamic actuator (elevator, canard, or elevon) δm, and the pitch thrust vectoring Δm:

$$F_Z + T_Z = \bar{q}S_{\text{ref}}(Cz_\alpha\alpha + Cz_{\delta m}\delta m) + T_\alpha\alpha + T_\Delta\Delta m \tag{7}$$

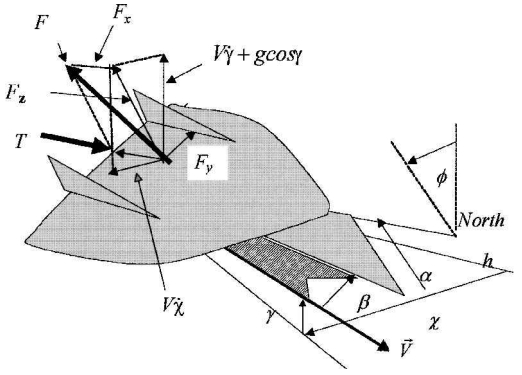

Fig. 1 Applied forces.

Combining Eqs. (3–7), one obtains

$$\dot{e}_\gamma = \dot{\gamma}^* + \frac{g\cos\gamma}{\text{vel}} - \frac{\bar{q}S_{\text{ref}}\cos\phi}{m\ \text{vel}}cz_{\delta m}\delta m - \frac{\cos\phi T_\Delta\Delta_m}{m\ \text{vel}} - \left(\frac{\bar{q}cz_\alpha S_{\text{ref}}}{m\ \text{vel}} + \frac{T}{m\ \text{vel}}\right)\alpha\cos\phi \tag{8}$$

$$\dot{e}_\chi = \dot{\chi}^* - \frac{\bar{q}S_{\text{ref}}\sin\phi}{m\ \text{vel}\cos\gamma}cz_{\delta m}\delta m - \frac{\sin\phi T_\Delta\Delta_m}{m\ \text{vel}\cos\gamma} - \left(\frac{\bar{q}cz_\alpha S_{\text{ref}}}{m\ \text{vel}\cos\gamma} + \frac{T}{m\ \text{vel}\cos\gamma}\right)\alpha\sin\phi \tag{9}$$

The direct contributions of δm and Δm to the flight-path and ground track motions in Eqs. (8) and (9) are small compared to that of the angle of attack; the flight-path and ground track motions are, therefore, governed by $\alpha\cos\phi$ and $\alpha\sin\phi$. The aircraft control problem can, thus, be divided into the following three subproblems, as represented by Fig. 2:

1) The autopilot outer-loop control problem consists of designing $u_\gamma = \hat{\alpha}\cos\hat{\phi}$ and $u_\chi = \hat{\alpha}\sin\hat{\phi}$, that is, designing the prescribed angle of attack and bank angles $\hat{\alpha}$ and $\hat{\phi}$ such that $e_\gamma \to 0$ and $e_\gamma \to 0$ asymptotically.

2) The inversion control problem consists of designing the prescribed attitude rates p^*, q^*, and r^*, the prescribed rolling, pitching, and yawing rates, respectively, such that $\alpha \to \hat{\alpha}$, $\phi \to \hat{\phi}$, and $\beta \to 0$ asymptotically.

This paper presents the application of linear-adaptive control methodology[15–18] to solving the outer-loop autopilot and inversion control problems, and subspace-stabilization techniques for the control of angular rates in the inner loop of control.

3) The inner-loop control problem consists of designing the deflections of roll, pitch, and yaw actuators δl, δm, and δn such that actual rolling, pitching, and yawing rates asymptotically track the prescribed attitude rates. That is, $p \to p^*$, $q \to q^*$, and $r \to r^*$.

This paper proposes using subspace-stabilization control techniques to achieve the required robustness in the control of the attitude rates.

Linear-Adaptive Autopilot

Examination of Eqs. (8) and (9) reveals several important points:

1) Equation (8) contains a nonlinear term.

2) The aerodynamic coefficients cz_α and cz_δ in Eqs. (8) and (9) vary with flight Mach number and are uncertain. Whereas relative model errors of 5–10% are common for aircraft, the relative error may reach 20–30% for RLV.

3) Measurements of the angle of attack α are not always easy, nor are they necessarily accurate.

4) In principle, it is easy to measure accurately the deflection of each of the control surfaces; measuring accurately the control

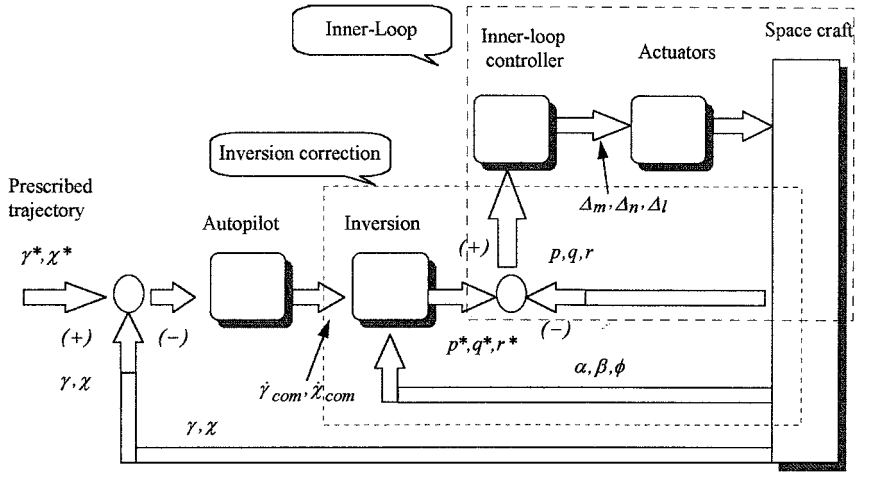

Fig. 2 Control architecture.

surface position, however, only solves part of the problem because the lift forces created by the actuator are roughly proportional to the sum of the actuator deflection and the local angle of attack, which may differ from the reference angle of attack due to downwash aerodynamic effects. In Eqs. (8) and (9), the effects of only a subset of variables are known, whereas the effects of each of the other variables are either too complicated or sufficiently uncertain to be taken into account in the design of the controller.

As pointed out in Ref. 15, the ultimate adaptive controller is a universal controller that does not require a priori, quantitative knowledge of the plant model's structure. Thus, an ultimate adaptive controller for the plant described by Eqs. (3) and (4) would only require the knowledge that the generic structure of the equation has the form

$$\dot{\gamma} = -(g/\text{vel})\cos\gamma - z_\gamma + b \cdot u_\gamma \tag{10}$$

where the structural form of the function $z_\gamma(\cdot)$ may be imperfectly known. This happens to be the case in flight control because the model in Eq. (8) is only an approximation of reality. In particular, not only are the effects of the variables δm and Δm imperfectly represented, but also the effects of other variables are not included. Given that each term and state variable of Eq. (8) can be written as the sum of the true value of the term, and given the error made on the modeling or the measurement of that term or variable, Eq. (8) can be rewritten as follows:

$$\begin{aligned}\dot{e}_\gamma &= -\frac{\bar{q}S_{\text{ref}}\cos\phi}{m\,\text{vel}}[\tilde{c}z_\alpha(\alpha+\tilde{\alpha}) + (cz_\delta + \tilde{c}z_\delta)(\delta m + \tilde{\delta}m) + cz_\alpha\tilde{\alpha}] \\ &\quad - \frac{[\tilde{T}(\alpha+\tilde{\alpha}) + T\tilde{\alpha}]\cos\phi}{m\,\text{vel}} - w + \dot{\gamma}^* + \frac{g}{\text{vel}}\cos\gamma - b_\gamma u_\gamma \\ b_\gamma u_\gamma &= \left(\frac{\bar{q}S_{\text{ref}}}{m\,\text{vel}} + \frac{T}{m\,\text{vel}}\right)\alpha\cos\phi\end{aligned} \tag{11}$$

where $\tilde{(\cdot)}$ represent either model errors or measurement errors and w is a disturbance representing the effects of all other variables not included in the model. As shown in Ref. 15, what one really needs to design an ideal universal adaptive controller is real-time knowledge of the combined time effects of all of the terms on the right side of Eq. (11), other than the terms bu_γ and $\dot{\gamma}^* + g\cos\gamma/\text{vel}$. The latter three terms represent, respectively, the effects of the control, the derivative of the prescribed flight-path angle, and the effects of a nonlinear term.

Linear-Adaptive Controller Design Technique

Following the linear-adaptive controller concept, as introduced in Refs. 15–17, the system flight-path and ground track response error can be represented as

$$\dot{e}_\gamma = \dot{\gamma}^* + z_\gamma + \frac{g}{\text{vel}}\cos\gamma - b_\gamma u_\gamma, \qquad b_\gamma = \frac{\bar{q}S_{\text{ref}}cz_\alpha}{m\,\text{vel}} + \frac{T}{m\,\text{vel}} \tag{12}$$

$$\dot{e}_\chi = \dot{\chi}^* + z_\chi - b_\chi u_\chi, \qquad b_\chi = \frac{1}{\cos\gamma}\left(\frac{\bar{q}S_{\text{ref}}cz_\alpha}{m\,\text{vel}} + \frac{T}{m\,\text{vel}}\right) \tag{13}$$

where the dependency of z_γ and z_χ on angle of attack, control terms, and velocity is omitted to simplify the notations. One of the key ideas of linear-adaptive control is to split the total control effort into three terms $u = u_{\text{nl}} + u_h + u_e$. The first control term u_{nl} compensates for the undesirable time-variation effects of known nonlinear terms, the second term u_h compensates for the combined time-variation effects of all uncertain terms and the third term u_e is a feedback control designed to achieve the prescribed error response. Thus,

$$u_{\gamma,\text{nl}} = (1/b_\gamma)[\dot{\gamma}^* + (g/\text{vel})\cos\gamma], \qquad u_{\gamma,h} = \hat{z}_\gamma/b_\gamma \tag{14}$$

$$u_{\chi,\text{nl}} = (1/b_\chi)\dot{\chi}^*, \qquad u_{\chi,h} = \hat{z}_\chi/b_\chi \tag{15}$$

Replacing $u_{(\cdot)} = u_{(\cdot),\text{nl}} + u_{(\cdot),h} + u_{(\cdot)e}$ and $(\cdot) = \gamma, \chi$ in Eqs. (12) and (13), and provided that the real-time estimations $\hat{z}_\gamma$ and $\hat{z}_\chi$ of the time variations of z_γ and z_χ are accurate enough, we obtain

$$\dot{e}_\gamma = z_\gamma - \hat{z}_\gamma - b_\gamma u_{\gamma,e} \approx -b_\gamma u_{\gamma,e} \tag{16}$$

$$\dot{e}_\chi = z_\chi - \hat{z}_\chi - b_\chi u_{\chi,e} \approx -b_\chi u_{\chi,e} \tag{17}$$

The desired ideal dynamic behavior of the error response, $e_{(\cdot)} = (\cdot)^* - (\cdot)$ and $(\cdot) = \gamma, \chi$ is embodied in the following ideal-model, which is assumed to be specified by the designer

$$\ddot{e}_{(\cdot)} + \zeta_{1,(\cdot)}\dot{e}_{(\cdot)} + \zeta_{0,(\cdot)}e_{(\cdot)} = 0, \qquad (\cdot) = \gamma, \chi \tag{18}$$

With the introduction of an additional state

$$\int_0^t e_{(\cdot)}\,\mathrm{d}\tau$$

representing the time integral of the tracking error, the application of this model to our flight-path equation, which is a first-order differential equation, leads to

$$\dot{e}_{(\cdot)} + \zeta_{1,(\cdot)}e_{(\cdot)} + \zeta_{0,(\cdot)}\int_0^t e_{(\cdot)}\,\mathrm{d}\tau = 0, \qquad (\cdot) = \gamma, \chi \tag{19}$$

Combining Eqs. (16–19) we obtain the final design of the controller. For the RLV application considered, the characteristic frequencies ϖ_γ and ϖ_χ of the prescribed flight-path angle and ground track response errors are chosen to be 0.2 and 0.04 rad/s, respectively. The gains in Eqs. (18) and (19) are $\zeta_{1,(\cdot)} = 1.4\varpi_{(\cdot)}$ and $\zeta_{0,(\cdot)} = \varpi_{(\cdot)}^2$.

Thus, the final idealized designs of the adaptive autopilot control laws are

$$u_\gamma = \hat{\alpha}\cos\hat{\phi} = b_\gamma^{-1}\left\{\dot{\gamma}^* + z_\gamma + \frac{g}{\text{vel}}\cos\gamma + 1.4\varpi_\gamma e_\gamma + \varpi_\gamma^2\int_0^t e_\gamma\,\mathrm{d}\tau\right\} \tag{20}$$

$$u_\chi = \hat{\alpha}\sin\hat{\phi} = b_\chi^{-1}\left\{\dot{\chi}^* + z_\chi + 1.4\varpi_\chi e_\gamma + \varpi_\chi^2\int_0^t e_\chi\,\mathrm{d}\tau\right\} \tag{21}$$

Disturbance Accommodation Observer

The next step in our autopilot design procedure is to incorporate a real-time disturbance observer, using the methods of disturbance-accommodating-control (DAC) theory.[15–18] For this purpose, the dynamics governing tracking errors can be written as follows

$$\dot{e}_\gamma = z_\gamma + U_\gamma \tag{22}$$

where

$$U_\gamma = \dot{\gamma}^* + g\cos\gamma/\text{vel} - b_\gamma u_\gamma \tag{23}$$

and

$$\dot{e}_\chi = z_\chi + U_\chi \tag{24}$$

$$U_\chi = \dot{\chi}^* - b_\chi \cdot u_\chi \tag{25}$$

The design of the DAC disturbance observer to estimate z_γ and z_χ follows the ideas presented in Refs. 15–18, where we will model the time behavior of the quantities to be estimated by a generalized spline model of the form

$$f[x(t)] = c_1 f_1(t) + \cdots + c_M f_M(t), \qquad i = 1, \ldots, M \tag{26}$$

where the set of known or chosen functions $\{f_i(t)\}$ constitutes a finite basis set and the set of weighting constants $\{c_i\}$ are unknown and may vary in time in an unknown, stepwise-constant manner, that is, jumps in the c_j values are sparse in time. Here, the basis functions $f_i(t)$ will be chosen as $f_1 = 1$, $f_2 = t$, and $f_3 = t^2$. In that case, Eqs. (22) and (25) can be represented by the generic model

$$\begin{aligned}\dot{y} &= z_1 + U, \qquad \dot{z}_1 = z_2 + \sigma_1(t) \\ \dot{z}_2 &= z_3 + \sigma_2(t), \qquad \dot{z}_3 = \sigma_3(t)\end{aligned} \tag{27}$$

where $z = (z_1, \ldots, z_3)^T$ is the state of $z_{(\cdot)}$ where $(\cdot) = \gamma, \chi$, and the $\sigma_i(t)$ are time sparse sequences of totally unknown impulses that mathematically model the uncertain jumps in the c_j in Eq. (26). Finally, the corresponding DAC-type disturbance observer algorithms for generating real-time estimates of the unknown states $z_1(t)$, $z_2(t)$, and $z_3(t)$ and the corresponding real-time tracking estimates $\hat{e}_\gamma$ and $\hat{e}_\chi$ are obtained from Ref. 15, page 1219, by writing

$$\dot{\hat{e}}_\gamma = \dot{\gamma}^* - \bar{\alpha}\cos\bar{\phi}\, b_\gamma + g\cos\gamma/V + \hat{z}_{1,\gamma} + k_1(e_\gamma - \hat{e}_\gamma)$$

$$\dot{\hat{z}}_{1,\gamma} = \hat{z}_{2,\gamma} + k_2(e_\gamma - \hat{e}_\gamma), \qquad \dot{\hat{z}}_{2,\gamma} = \hat{z}_{3,\gamma} + k_3(e_\gamma - \hat{e}_\gamma)$$

$$\dot{\hat{z}}_{3,\gamma} = k_4(e_\gamma - \hat{e}_\gamma) \tag{28}$$

$$\dot{\hat{e}}_\chi = \dot{\chi}^* - \bar{\alpha}\sin\bar{\phi}\, b_\chi + \hat{z}_{1,\chi} + k_1(e_\chi - \hat{e}_{1,\chi})$$

$$\dot{\hat{z}}_{1,\chi} = \hat{z}_{2,\chi} + k_2(e_\chi - \hat{e}_{1,\chi}), \qquad \dot{\hat{z}}_{2,\chi} = \hat{z}_{3,\chi} + k_3(e_\chi - \hat{e}_{1,\chi})$$

$$\dot{\hat{z}}_{3,\chi} = k_4(e_\chi - \hat{e}_{1,\chi}) \tag{29}$$

For our RLV application, the eigenvalues for the flight-path observers will be chosen as $\lambda_j = -50$ and $j = 1, 4$ and the corresponding gains are $k_1 = 200$, $k_2 = 15{,}000$, $k_3 = 500{,}000$, and $k_4 = 6{,}250{,}000$. Choosing for the ground track observer an integral of time multiplied by absolute error (ITAE) type[19] ramp-input law with a characteristic frequency response of 50 rad/s, the gains are $k_1 = 120$, $k_2 = 12{,}325$, $k_3 = 676{,}250$, and $k_4 = 6{,}250{,}000$. The controls generated by the autopilot can, therefore, be written as the following practical realization of the idealized adaptive controllers in Eqs. (20) and (21)

$$u_\gamma = \bar{\alpha}\cos\bar{\phi} = b_\gamma^{-1}\left\{\dot{\gamma}^* + \hat{z}_{1,\gamma} + \frac{g}{\text{vel}}\cos\gamma + 1.4\varpi_\gamma e_\gamma + \varpi_\gamma^2\int_0^t e_\gamma\, d\tau\right\} \tag{30}$$

$$u_\chi = \bar{\alpha}\sin\bar{\phi} = b_\chi^{-1}\left\{\dot{\chi}^* + \hat{z}_{1,\chi} + 1.4\varpi_\chi e_\gamma + \varpi_\chi^2\int_0^t e_\chi\, d\tau\right\} \tag{31}$$

New Inversion Technique

Analytical Inversion

Let us assume, initially, that the following simplifying assumptions are valid:

1) The lift produced by aerodynamic and propulsive effects is directly proportional to the coordinated angle of attack $\bar{\alpha}$. This means that the effects of actuator deflections from trim conditions are essentially zero. Although this assumption might be valid when averaged over the entire flight, it is not necessarily valid at each moment of time.

2) The value of the coefficient $b_\gamma = (\bar{q}S_{\text{ref}}cz_\alpha + T)/m\,\text{vel}$ is known perfectly. This we know is not necessarily the case in practice.

3) The resultant force lies in the plane of symmetry of the aircraft and the sideslip angle is regulated to zero. Should this not be the case, the effects of a transversal lift proportional to $\beta\sin\phi$ would add a term to the flight-path equation and the effects of a transversal lift proportional to $\beta\cos\phi$ would add a term to the ground track equation.

The proposed analytical inversion procedure is as follows:

1) The angle of attack $\bar{\alpha}$ and bank angle $\bar{\phi}$ are calculated using condition (2), that is,

$$\bar{\phi} = \tan^{-1}(\hat{u}_\chi/\hat{u}_\gamma) \tag{32}$$

where when the skid-to-turn mode is chosen, Eq. (32) is replaced by $\bar{\phi} = 0$. In both cases the corresponding angle of attack is given by

$$\bar{\alpha} = \hat{u}_\gamma\cos\bar{\phi} + \hat{u}_\chi\sin\bar{\phi} \tag{33}$$

2) Real-time observers are used to estimate $\dot{\bar{\alpha}}$ and $\dot{\bar{\phi}}$. The corresponding estimated variables are denoted by $\hat{\bar{\alpha}}$, $\hat{\bar{\phi}}$, $\dot{\hat{\bar{\alpha}}}$, and $\dot{\hat{\bar{\phi}}}$.

3) In the case of the turn-to-bank autopilot, the prescribed trajectory angles and their derivatives and the estimated angle of attack and bank angle and their derivatives are used to calculate the prescribed pitch and yaw Euler angles, θ_c and ψ_c, which can be approximated by

$$\theta_c = \gamma^* + \sin^{-1}(\bar{\alpha}\cos\bar{\phi} + \bar{\beta}\sin\bar{\phi}) \tag{34}$$

$$\psi_c = \chi^* + \tan^{-1}\left(\frac{\bar{\alpha}\sin\bar{\phi} - \bar{\beta}\cos\phi}{\cos\theta_c}\right) \tag{35}$$

The third Euler angle is the bank angle already calculated. Notwithstanding the prescribed value $\bar{\beta} \equiv 0$ of the sideslip angle, we keep $\bar{\beta}$ explicit in Eqs. (34) and (35) to cover extended cases where a nonzero sideslip angle may be prescribed and to introduce later the inversion error corrector scheme adopted. The time derivatives of θ_c and ψ_c are

$$\dot{\theta}_c = \dot{\gamma}^* + \frac{\dot{\bar{\alpha}}\cos\bar{\phi} - \bar{\alpha}\dot{\bar{\phi}}\sin\bar{\phi} + \dot{\bar{\beta}}\sin\bar{\phi} - \bar{\beta}\cos\bar{\phi}\dot{\bar{\phi}}}{[1 - (\bar{\alpha}\cos\bar{\phi} + \bar{\beta}\sin\bar{\phi})^2]^{0.5}} \tag{36}$$

$$\dot{\psi}_c = \dot{\chi}^* + \frac{\cos\theta_c(\dot{\bar{\alpha}}\sin\bar{\phi} + \bar{\alpha}\dot{\bar{\phi}}\cos\bar{\phi} - \dot{\bar{\beta}}\cos\bar{\phi} + \bar{\beta}\sin\phi\dot{\phi}) + \sin\theta_c\dot{\theta}_c(\bar{\alpha}\sin\bar{\phi} - \bar{\beta}\cos\bar{\phi})}{\cos\theta_c^2 + (\bar{\alpha}\sin\bar{\phi} - \bar{\beta}\cos\bar{\phi})^2} \tag{37}$$

4) In the case of the skid-to-turn autopilot, $\bar{\phi}$ and $\dot{\bar{\phi}} = 0$ in Eqs. (34–36) and

$$\dot{\psi}_c = \dot{\chi}^* + \cos\theta_c\hat{u}_\chi \tag{38}$$

Equations (34–38) include $\dot{\bar{\alpha}}$ and $\dot{\bar{\phi}}$, the time derivatives of prescribed angle of attack angle and prescribed bank angle. The method used in Refs. 7 and 8 to calculate those quantities is to filter $\bar{\alpha}$ and $\bar{\phi}$. That method permits one to introduce desired flying qualities and to calculate corresponding first derivatives of filtered signals. The selection of that filter's response characteristic frequency must seek a compromise between a sufficiently fast response and acceptable noise levels. The characteristic frequencies of the angle of attack and bank angle filters were chosen to be 2 and 1 rad/s, respectively. Assuming that $\hat{\bar{\alpha}}$ and $\hat{\bar{\beta}}$ are small and that $|\theta_c|$ is smaller than 80 deg, one can rewrite Eqs. (36–38) with the expressions for the estimated states and obtain

$$\dot{\theta}_c = \dot{\gamma}^* + \dot{\hat{\bar{\alpha}}}\cos\hat{\bar{\phi}} - \hat{\bar{\alpha}}\dot{\hat{\bar{\phi}}}\sin\hat{\bar{\phi}} + \dot{\bar{\beta}}\sin\hat{\bar{\phi}} - \bar{\beta}\cos\hat{\bar{\phi}}\dot{\hat{\bar{\phi}}} \tag{39}$$

$$\dot{\psi}_c = \dot{\chi}^* + \frac{\dot{\hat{\bar{\alpha}}}\sin\hat{\bar{\phi}} + \hat{\bar{\alpha}}\cdot\dot{\hat{\bar{\phi}}}\cos\hat{\bar{\phi}} - \dot{\bar{\beta}}\cos\hat{\bar{\phi}}}{\cos\theta_c} + \frac{\tan\theta_c}{\cos\theta_c}(\hat{\bar{\alpha}}\sin\hat{\bar{\phi}} - \bar{\beta}\cos\hat{\bar{\phi}})\dot{\theta}_c \tag{40}$$

The inner loop of control tracks the roll rate, pitch rate, and yaw rate commands $\breve{p}$, $\breve{q}$, and $\breve{r}$ as generated by the inversion procedure using the following equations

$$\breve{p} = \dot{\hat{\bar{\phi}}} - \dot{\psi}_c\sin\hat{\theta} \tag{41}$$

$$\breve{q} = \dot{\psi}_c\sin\hat{\bar{\phi}}\cos\hat{\theta} + \dot{\theta}_c\cos\hat{\bar{\phi}} \tag{42}$$

$$\breve{r} = \dot{\psi}_c\cos\hat{\bar{\phi}}\cos\hat{\theta} - \dot{\theta}_c\sin\hat{\bar{\phi}} \tag{43}$$

where $\breve{p}, \breve{q}$, and $\breve{r}$ are the prescribed inner-loop profiles, if we assume a perfect inversion. We will now show how to correct inversion errors.

Correction of Inversion Errors

Calculation of the prescribed angle of attack $\hat{\alpha}$ and of the prescribed bank angle $\hat{\phi}$ is based on the simplifying assumptions that 1) the lift is solely proportional to the prescribed angle of attack, 2) the corresponding lift gradient is exact, and 3) the resulting force lies perfectly in the symmetry plane. Those assumptions are not exactly satisfied in practice. Because the relation between pitching, rolling, and yawing rates and Euler angles is holonomic, their transformation should not involve any error. Therefore, any errors that appear in the inversion will be associated with the aerodynamic angles. Suppose the time evolutions of the inversion errors are modeled by the generic differential equation

$$\begin{bmatrix} \delta\dot{\alpha} \\ \delta\dot{\beta} \\ \delta\dot{\phi} \end{bmatrix} = \boldsymbol{F}(\delta\alpha, \delta\beta, \delta\phi, \alpha, \phi, p, q, r, \gamma, \dot{\gamma}, \dot{\chi}, \delta m, \delta n, \delta l) + \boldsymbol{B}\begin{bmatrix} \delta q \\ \delta r \\ \delta p \end{bmatrix}$$

$$\begin{bmatrix} \delta\alpha \\ \delta\beta \\ \delta\phi \end{bmatrix} = \begin{bmatrix} \hat{\alpha} - \alpha \\ 0 - \beta \\ \hat{\phi} - \phi \end{bmatrix} \tag{44}$$

where $[\delta q \;\; \delta r \;\; \delta p]^T$ is an inversion correction term to be added to the inner loop's prescribed pitch, roll, and yaw rate profiles, so that the inner loop actually tracks $[\breve{q} + \delta q, \breve{r} + \delta r, \breve{p} + \delta p]^T$. The following differential equations will be used to model, in velocity axis, the behavior of the angle of attack α, the sideslip angle β, and the bank angle ϕ:

$$\dot{\alpha} = q - (p\cos\alpha + r\sin\alpha)\tan\beta - \frac{\cos\phi}{\cos\beta}\dot{\gamma} - \frac{\sin\phi\cos\gamma}{\cos\beta}\dot{\chi} \tag{45}$$

$$\dot{\beta} = p\sin\alpha - \cos\alpha - \sin\phi\dot{\gamma} + \cos\phi\cos\gamma\dot{\chi} \tag{46}$$

$$\dot{\phi} = \frac{\cos\alpha}{\cos\beta}p + \frac{\sin\alpha}{\cos\beta}r + \tan\beta\cos\phi\dot{\gamma} + [\sin\gamma + \tan\beta\sin\phi\cos\gamma]\dot{\chi} \tag{47}$$

We do not need to derive the explicit expression for the vector $\boldsymbol{F}$ in Eq. (44). Rather, it is only necessary to derive the matrix $\boldsymbol{B}$ representing the effects that corrections δq, δq, and δr have on the evolution of the errors. Using Eqs. (45–47), we obtain, in the neighborhood of the prescribed turn conditions,

$$\begin{bmatrix} \delta\dot{\alpha} \\ \delta\dot{\beta} \\ \delta\dot{\phi} \end{bmatrix} = \boldsymbol{F} + \boldsymbol{B}\begin{bmatrix} \delta q \\ \delta r \\ \delta p \end{bmatrix}$$

$$\boldsymbol{B} = \begin{bmatrix} 1 & 0 & 0 \\ 0 & -\cos\hat{\alpha} & \sin\hat{\alpha} \\ \sin\hat{\phi}\tan\theta_c & \cos\hat{\phi}\tan\theta_c & 1 \end{bmatrix} \tag{48}$$

For the representative RLV flight profile used in our simulation, with $|\phi| < \pi/2$ and the combined value of $\alpha(t)$ and $\theta(t)$, the matrix $\boldsymbol{B}$ turns out to be always invertible. Designating by $[\hat{z}_{1\alpha} \;\; \hat{z}_{1\beta} \;\; \hat{z}_{1\phi}]^T$ the real-time estimation of the three-vector $\boldsymbol{F}$ in Eq. (44), the vector correction term $[\delta q \;\; \delta r \;\; \delta p]^T$, which cancels the effects of $\boldsymbol{F}$ in Eq. (44) and achieves the prescribed behavior of the inversion errors, is obtaining by solving Eq. (48) and is given by

$$\begin{bmatrix} \delta q \\ \delta r \\ \delta p \end{bmatrix} = \boldsymbol{B}^{-1}\begin{bmatrix} \alpha_{\text{cor}} \\ \beta_{\text{cor}} \\ \phi_{\text{cor}} \end{bmatrix}$$

$$\begin{bmatrix} \alpha_{\text{cor}} \\ \beta_{\text{cor}} \\ \phi_{\text{cor}} \end{bmatrix} = -\begin{bmatrix} \hat{z}_{1,\alpha} \\ \hat{z}_{1,\beta} \\ \hat{z}_{1,\phi} \end{bmatrix} + \begin{bmatrix} -a_1\delta\alpha - a_0\displaystyle\int_0^t \delta\alpha\,\mathrm{d}\tau \\ -b_1\delta\beta - b_0\displaystyle\int_0^t \delta\beta\,\mathrm{d}\tau \\ -d_1\delta\phi - d_0\displaystyle\int_0^t \delta\phi\,\mathrm{d}\tau \end{bmatrix} \tag{49}$$

Introduction of the Correction

Although, in principle, one could introduce the inversion error corrections as additive terms to the prescribed pitch, roll, and yaw rates as described, the drawback of that approach is that it would introduce a discrepancy between the calculated and actual Euler angles. In this subsection we will show that the same correction can be achieved by substituting $[\hat{\dot{\alpha}} + \alpha_{\text{cor}} \;\; \hat{\dot{\beta}} + \beta_{\text{cor}} \;\; \hat{\dot{\phi}} + \phi_{\text{cor}}]^T$ for $[\hat{\dot{\alpha}} \;\; \hat{\dot{\beta}} \;\; \hat{\dot{\phi}}]^T$ in Eqs. (39) and (40), where the corresponding observer states and the nullity of the prescribed sideslip angle are introduced to replace the prescribed angle of attack and bank angle terms. We will demonstrate that this latter formulation satisfies

$$\begin{bmatrix} \delta\dot{\alpha} \\ \delta\dot{\beta} \\ \delta\dot{\phi} \end{bmatrix} = \begin{bmatrix} -a_1\delta\alpha - a_0\displaystyle\int_0^t \delta\alpha\,\mathrm{d}\tau \\ -b_1\delta\beta - b_0\displaystyle\int_0^t \delta\beta\,\mathrm{d}\tau \\ -d_1\delta\phi - d_0\displaystyle\int_0^t \delta\phi\,\mathrm{d}\tau \end{bmatrix} \tag{50}$$

$$\delta\dot{\theta}_c = \alpha_{\text{cor}}\cos\hat{\phi} - \hat{\alpha}\cdot\phi_{\text{cor}}\sin\hat{\phi} + \beta_{\text{cor}}\sin\hat{\phi} \tag{51}$$

$$\delta\dot{\psi}_c = \frac{\alpha_{\text{cor}}\sin\hat{\phi} + \hat{\alpha}\phi_{\text{cor}}\cos\hat{\phi} - \beta_{\text{cor}}\cos\hat{\phi}}{\cos\theta_c} + \frac{\tan\theta_c}{\cos\theta_c}(\hat{\alpha}\sin\hat{\phi})\delta\dot{\theta}_c \tag{52}$$

This is demonstrated by combining Eqs. (41–43) and (51) and (52) and assuming that $\hat{\alpha}\tan\theta_c$ is small (either because large pitch angles imply that the angle of attack is small or because large angles of attack are associated with relatively small pitch angles) and leads to the result

$$\begin{bmatrix} \delta q \\ \delta r \\ \delta p \end{bmatrix} = \boldsymbol{D}\begin{bmatrix} \alpha_{\text{cor}} \\ \beta_{\text{cor}} \\ \phi_{\text{cor}} \end{bmatrix}, \qquad \boldsymbol{D} = \begin{bmatrix} 1 & 0 & 0 \\ 0 & -1 & \hat{\alpha} \\ \sin\hat{\phi}\tan\theta_c & -\cos\hat{\phi}\tan\theta_c & 1 \end{bmatrix} \tag{53}$$

For small angles of attack we have $\boldsymbol{D} = \boldsymbol{B}^{-1}$, which establishes that at the end of the settling time of the observers, which estimate the time variations of the vector $\boldsymbol{F}$, Eq. (48) can be written as

$$\begin{bmatrix} \delta\dot{\alpha} \\ \delta\dot{\beta} \\ \delta\dot{\phi} \end{bmatrix} = \boldsymbol{F} + \boldsymbol{B}\boldsymbol{B}^{-1}\left[-\begin{bmatrix} \hat{z}_{1,\alpha} \\ \hat{z}_{1,\beta} \\ \hat{z}_{1,\phi} \end{bmatrix} + \begin{bmatrix} -a_1\delta\alpha - a_0\displaystyle\int_0^t \delta\alpha\,\mathrm{d}\tau \\ -b_1\delta\beta - b_0\displaystyle\int_0^t \delta\beta\,\mathrm{d}\tau \\ -d_1\delta\phi - d_0\displaystyle\int_0^t \delta\phi\,\mathrm{d}\tau \end{bmatrix}\right]$$

$$\Rightarrow \begin{bmatrix} \delta\dot{\alpha} \\ \delta\dot{\beta} \\ \delta\dot{\phi} \end{bmatrix} \approx \begin{bmatrix} -a_1\delta\alpha - a_0\displaystyle\int_0^t \delta\alpha\,\mathrm{d}\tau \\ -b_1\delta\beta - b_0\displaystyle\int_0^t \delta\beta\,\mathrm{d}\tau \\ -d_1\delta\phi - d_0\displaystyle\int_0^t \delta\phi\,\mathrm{d}\tau \end{bmatrix} \tag{54}$$

In the RLV application considered here, the eigenvalues associated with the error responses of the corrections of the angle of attack, the sideslip angle, and the bank angle are chosen to be $\lambda_{\phi,1/2} = \lambda_{\beta,1/2} - 0.7 \pm i0.7$ and $\lambda_{\alpha,1/2} = -1.4 \pm i1.4$. Consequently, $b_0 = d_0 = 1$ and $b_1 = d_1 = 1.4$ and $a_0 = 4$ and $a_1 = 2.8$ in Eq. (54).

Rewriting Eqs. (41–43) with the new entries

$$[\hat{\dot{\alpha}} + \alpha_{\text{cor}} \quad \hat{\dot{\beta}} + \beta_{\text{cor}} \quad \hat{\dot{\phi}} + \phi_{\text{cor}}]^T$$

leads to the following expressions for the correction controls:

$$p^* = \breve{p} + \delta\rho = \hat{\dot{\phi}} + \phi_{\text{cor}} - (\dot{\psi}_c + \delta\dot{\psi}_c)\sin\hat{\theta} \tag{55}$$

$$q^* = \breve{q} + \delta q = (\dot{\psi}_c + \delta\dot{\psi}_c)\sin\hat{\phi}\cos\hat{\theta} + (\dot{\theta}_c + \delta\dot{\theta}_c)\cos\hat{\phi} \quad (56)$$

$$r^* = \breve{r} + \delta r = (\dot{\psi}_c + \delta\dot{\psi}_c)\cos\hat{\phi}\cos\hat{\theta} - (\dot{\theta}_c + \delta\dot{\theta}_c)\sin\hat{\phi} \quad (57)$$

where $\delta\dot{\theta}_c$ and $\delta\dot{\psi}_c$ are defined by Eqs. (51) and (52).

Real-Time Estimation of Uncertain Terms in Inversion Error Dynamics

A set of DAC observers that estimate $z_{(\cdot)}$ where $(\cdot) = \alpha, \beta, \phi$ can be derived using Eq. (48). For this purpose, the prescribed characteristic equation common to all three observers is based on an ITAE optimal characteristic polynomial[19] with a characteristic frequency $\omega_{(\cdot)}$ where $(\cdot) = \alpha, \beta, \phi$ of 7 rad/s. The final forms of those three observers are

$$\begin{bmatrix} \delta\dot{\hat{\alpha}} \\ \dot{\hat{z}}_{1,\alpha} \\ \dot{\hat{z}}_{2,\alpha} \end{bmatrix} = \begin{bmatrix} \hat{z}_{1,\alpha} + ko_{1,\alpha}(\delta\alpha - \delta\hat{\alpha}) + \delta q \\ \hat{z}_{2,\alpha} + ko_{2,\alpha}(\delta\alpha - \delta\hat{\alpha}) \\ ko_{3,\alpha}(\delta\alpha - \delta\hat{\alpha}) \end{bmatrix} \quad (58)$$

$$\begin{bmatrix} \delta\dot{\hat{\beta}} \\ \dot{\hat{z}}_{1,\beta} \\ \dot{\hat{z}}_{2,\beta} \end{bmatrix} = \begin{bmatrix} \hat{z}_{1,\beta} + ko_{1,\beta}(\delta\beta - \delta\hat{\beta}) + \sin\hat{\alpha}\delta p - \cos\hat{\alpha}\delta r \\ \hat{z}_{2,\beta} + ko_{2,\beta}(\delta\beta - \hat{\beta}) \\ ko_{3,\beta}(\delta\beta - \hat{\beta}) \end{bmatrix} \quad (59)$$

$$\begin{bmatrix} \delta\dot{\hat{\phi}} \\ \dot{\hat{z}}_{1,\phi} \\ \dot{\hat{z}}_{2,\phi} \end{bmatrix} = \begin{bmatrix} \hat{z}_{1,\phi} + ko_{1,\phi}(\delta\phi - \delta\hat{\phi}) + \delta p + \sin\hat{\phi}\tan\theta_c\delta q + \cos\hat{\phi}\tan\theta_c \cdot \delta r \\ \hat{z}_{2,\phi} + ko_{2,\phi}(\delta\beta - \hat{\beta}) \\ ko_{3,\phi}(\delta\beta - \hat{\beta}) \end{bmatrix} \quad (60)$$

Note that Eqs. (48), (52), and (53) contain the term $\tan\theta_c$. As a consequence, Eq. (60) has a singularity for the value $\theta_c = \pm\pi/2$. This type of difficulty can be overcome using quaternions. However, the inconvenience of such an approach is that it complicates even more a formulation of the equations that is already rather complicated. Because such singularity terms appear only in the correction of the errors, the remedy we use here is to restrict application of the inversion correction to those cases when the value of θ_c in Eqs. (48) and (52) is smaller than 80 deg. This imposed limitation appears during the first 60 s in the mission just after vertical launch, where the bank angle is still zero, and, therefore, the need for correcting bank error has not yet appeared.

Inner-Loop Control Design

The design of the inner loop of control utilizes the subspace-stabilization technique.[20,21] This control design technique provides the desired robustness in the inner loop that controls rolling, pitching, and yawing rates. It also serves to effectively decouple the control of each axis from the disturbing effects of the coupling terms from the other axis. The design of each of the three channels is identical, so we shall illustrate it by considering only the pitching rate. For this purpose, with linear-adaptive control ideas, the equation that describes the pitching rate[6] error response $e_q = (q^* - q)$ can be written as $\dot{e}_q = \dot{q}^* - m[\boldsymbol{x}(t)] + M_m\Delta_m$, where q^* represents the prescribed pitching rate, $m[\boldsymbol{x}(t)]$ represents the combined effect of all other terms in the error response other that the terms involving the pitch thrust vectoring $M_m\Delta_m$, where the symbol $M_m = \partial\dot{q}/\partial\Delta_m$ and Δ_m represents thrust-vectoring deflections. With the introduction of the disturbance $z_{1,q}$, the pitching rate error response can be written as

$$\dot{e}_q = z_{1,q} + M_m\Delta_m, \qquad z_{1,q} = \dot{q}^* - m[x(t)] \quad (61)$$

where the actuator response is represented by

$$\dot{\Delta}_m = -\varpi\Delta_m + \varpi u_q \quad (62)$$

A quadratic polynomial-spline waveform model, as used in Eq. (28), was used to represent the time behavior of the uncertain term $z_{1,q}$ in Eq. (62). A DAC disturbance observer was then designed as discussed earlier and has the following form

$$\dot{\hat{e}}_q = M_m + \hat{z}_{1,q} + k_1(e_q - \hat{e}_q), \qquad \dot{\hat{z}}_{1,q} = \hat{z}_{2,q} + k_2(e_q - \hat{e}_q)$$

$$\dot{\hat{z}}_{2,q} = \hat{z}_{3,q} + k_3(e_q - \hat{e}_q), \qquad \dot{\hat{z}}_{3,q} = k_4(e_q - \hat{e}_q) \quad (63)$$

For our application, we chose the observer error eigenvalues associated with Eq. (63) to be $\lambda_i = -50$, $i = 1, \ldots, 4$, which correspond to $k_1 = 200$, $k_2 = 15{,}000$, $k_3 = 500{,}000$, and $k_4 = 6{,}250{,}000$.

The three state variables were chosen as the time integral of the tracking error, the tracking error, and its first time derivative. Thus, Eqs. (61) and (62) are written as

$$\begin{bmatrix} \dot{x}_1 \\ \dot{x}_2 \\ \dot{x}_3 \end{bmatrix} = \begin{bmatrix} 0 & 1 & 0 \\ 0 & 0 & 1 \\ 0 & 0 & -\varpi \end{bmatrix} \begin{bmatrix} x_1 \\ x_2 \\ x_3 \end{bmatrix} + \begin{bmatrix} 0 \\ 0 \\ z_{2,q} + \varpi z_{2,q} + \varpi M_m u_{\mathrm{nl}} \end{bmatrix} + \begin{bmatrix} 0 \\ 0 \\ \varpi M_m u_e \end{bmatrix} \quad (64)$$

where

$$\boldsymbol{x} = \{x_1, x_2, x_3\} = \left\{ \int_0^t e_q \, \mathrm{d}\tau, e_q, \dot{e}_q \right\}$$

$e_q = q^* - q$, and ϖ represents the characteristic frequency of the first-order response of the actuator.

Subspace Stabilization

The main control objectives required to effectively achieve a satisfactory error response are 1) prompt regulation of the system state $\boldsymbol{x}(t)$ to the prescribed value $\boldsymbol{x}(t)^*$ generated by the aforementioned filters, that is, $\boldsymbol{x}(t) \to \boldsymbol{x}(t)^*$ as $t \to \infty$, and 2) as $\boldsymbol{x}(t)$ approaches $\boldsymbol{x}(t)^*$, maintain an acceptable error response in accordance with a specified ideal model differential equation such as

$$\ddot{e} + \alpha_1\dot{e} + \alpha_0 e = 0, \qquad e = (\cdot)^* - (\cdot), \qquad (\cdot) = q, p, r \quad (65)$$

where $(\cdot)^*$ and $(\cdot)$ are, respectively, the prescribed and actual behaviors of the system outputs we want to control. The prescribed values of α_1 and α_0 embody the desired automatic pilot settling time, overshoot, damping, and other requirements. The subspace-stabilization control technique introduced in Ref. 20 has opened up the possibility of achieving significant improvements in regulation and servo-tracking control problems. Using that technique, we design the controller to obtain a prescribed error response according to objective 2, which then guarantees the fulfillment of objective 1. For that purpose, a subspace of the system error space, representing the desired behavior of the error time response, is defined, and the control is then designed to stabilize $e(t)$ to that prescribed subspace in error space.

Brief Summary of the Subspace-Stabilization Control Technique[20,21]

Let $\boldsymbol{E}^n$ be the n-dimensional Euclidean space of coordinates $\{x_1, x_2, \ldots, x_n\}$ and let $\boldsymbol{S} \subset \boldsymbol{E}^n$ be the p-dimensional subspace spanned by a given set of p linearly independent vectors $\{m_1, m_2, \ldots, m_p\}$.

The (linear) subspace-stabilization control problem is to find a feedback control $\boldsymbol{u} = \boldsymbol{K}\boldsymbol{x}$ such that all solutions $\boldsymbol{x}(t)$ of the closed-loop system $\dot{\boldsymbol{x}} = \boldsymbol{A}\boldsymbol{x} + \boldsymbol{B}\boldsymbol{K}\boldsymbol{x}$ asymptotically approach $\boldsymbol{S}$ as $t \to \infty$ and such that all motions $\boldsymbol{x}(t) \in \boldsymbol{S}$ satisfy prescribed boundedness or stability conditions. For our application, the surface $\boldsymbol{S}$ represents the desired time behavior of the error state components in Eqs. (65) and is defined for each control channel, by an expression of the form

$$\boldsymbol{S}_{(\cdot)} : [\alpha_0, \alpha_1, 1] \begin{bmatrix} x_{1,(\cdot)} \\ x_{2,(\cdot)} \\ x_{3,(\cdot)} \end{bmatrix} = 0, \qquad (\cdot) = p, q, r \quad (66)$$

The essential mathematical features of the subspace-stabilization control problem and its solution become clear when viewed in a certain transformed coordinate system $\boldsymbol{x} \to (\boldsymbol{\xi}_1, \boldsymbol{\xi}_2)^T$ where the norm of the subvector $\boldsymbol{\xi}_1 \in \boldsymbol{R}^1$ constitutes a measure of the distance to the subspace $\boldsymbol{S}$ and the subvector $\boldsymbol{\xi}_2 \in \boldsymbol{R}^2$ represents the motion of the error state on the subspace $\boldsymbol{S}$. The system model is transformed from the original $\boldsymbol{x}$ coordinates to the $\boldsymbol{\xi}$ coordinates using a special nonsingular transformation[20] that projects the system state $\boldsymbol{x}$ into a component $\boldsymbol{C}\#\boldsymbol{\xi}_1$ perpendicular (orthogonal) to the subspace $\boldsymbol{S}$ and a component $\boldsymbol{M}\boldsymbol{\xi}_2$ lying in the subspace $\boldsymbol{S}$.

Because the given matrix $\boldsymbol{M} = \{\boldsymbol{m}_1, \boldsymbol{m}_2, \ldots, \boldsymbol{m}_p\}$ consists of p linearly independent columns, $\text{Rank}(\boldsymbol{M}) = p$. Let $\boldsymbol{C}$ be any $(n - p) \times n$ matrix having rank $(n - p)$, such that $\boldsymbol{CM} = \boldsymbol{0}$. The transformation from the $\boldsymbol{x}$ system to the new $\boldsymbol{\xi}$ system is defined by[20]

$$\boldsymbol{x} = [\boldsymbol{C}\# \mid \boldsymbol{M}]\begin{bmatrix}\boldsymbol{\xi}_1 \\ \hline \boldsymbol{\xi}_2\end{bmatrix}, \qquad \boldsymbol{\xi} = \begin{bmatrix}\boldsymbol{\xi}_1 \\ \hline \boldsymbol{\xi}_2\end{bmatrix} = \begin{bmatrix}\boldsymbol{C} \\ \hline \boldsymbol{M}\#\end{bmatrix}\boldsymbol{x}$$

$$\boldsymbol{C}\# = \boldsymbol{C}^T(\boldsymbol{C}^T\boldsymbol{C})^{-1}, \qquad \boldsymbol{M}\# = (\boldsymbol{M}^T\boldsymbol{M})^{-1}\boldsymbol{M}^T \tag{67}$$

We will consider the linear, state-feedback control law $\boldsymbol{u} = \boldsymbol{K}_e\boldsymbol{x}$ where $\boldsymbol{K}_e$ is to be designed to achieve prompt stabilization of $\boldsymbol{x}(t)$ to the subspace $\boldsymbol{S}$.

In the new ξ space the original state equation $\dot{\boldsymbol{x}} = \boldsymbol{Ax} + \boldsymbol{Bu}$ is transformed to the block system

$$\begin{bmatrix}\dot{\boldsymbol{\xi}}_1 \\ \hline \dot{\boldsymbol{\xi}}_2\end{bmatrix} = \left[\begin{array}{c|c} \boldsymbol{CAC}\# - \boldsymbol{C}\dot{\boldsymbol{C}}\# + \boldsymbol{CBK}_e\boldsymbol{C}\# & \boldsymbol{CAM} - \boldsymbol{C}\dot{\boldsymbol{M}} + \boldsymbol{CBK}_e\boldsymbol{M} \\ \hline \boldsymbol{M}\#\boldsymbol{AC}\# - \boldsymbol{M}\#\dot{\boldsymbol{C}}\# + \boldsymbol{M}\#\boldsymbol{BK}_e\boldsymbol{C}\# & \boldsymbol{M}\#\boldsymbol{AM} - \boldsymbol{M}\#\dot{\boldsymbol{M}} + \boldsymbol{M}\#\boldsymbol{BK}_e\boldsymbol{M}\end{array}\right]\begin{bmatrix}\boldsymbol{\xi}_1 \\ \hline \boldsymbol{\xi}_2\end{bmatrix} \tag{68}$$

which can written compactly as

$$\begin{bmatrix}\dot{\boldsymbol{\xi}}_1 \\ \hline \dot{\boldsymbol{\xi}}_2\end{bmatrix} = \left[\begin{array}{c|c} \bar{\boldsymbol{A}}_{11} + \bar{\boldsymbol{B}}_1\bar{\boldsymbol{K}}_1 & \bar{\boldsymbol{A}}_{12} + \bar{\boldsymbol{B}}_1\bar{\boldsymbol{K}}_2 \\ \hline \bar{\boldsymbol{A}}_{21} + \bar{\boldsymbol{B}}_2\bar{\boldsymbol{K}}_1 & \bar{\boldsymbol{A}}_{22} + \bar{\boldsymbol{B}}_2\bar{\boldsymbol{K}}_2\end{array}\right]\begin{bmatrix}\boldsymbol{\xi}_1 \\ \hline \boldsymbol{\xi}_2\end{bmatrix} \tag{69}$$

where

$$\bar{\boldsymbol{A}}_{11} = \boldsymbol{CAC}\# - \boldsymbol{C}\dot{\boldsymbol{C}}\#, \qquad \bar{\boldsymbol{B}}_1 = \boldsymbol{CB}, \qquad \bar{\boldsymbol{A}}_{12} = \boldsymbol{CAM} - \boldsymbol{C}\dot{\boldsymbol{M}}$$

$$\bar{\boldsymbol{A}}_{21} = \boldsymbol{M}\#\boldsymbol{AC}\# - \boldsymbol{M}\#\dot{\boldsymbol{C}}\#, \qquad \bar{\boldsymbol{A}}_{22} = \boldsymbol{M}\#\boldsymbol{AM} - \boldsymbol{M}\#\dot{\boldsymbol{M}}\#$$

$$\bar{\boldsymbol{B}}_2 = \boldsymbol{M}\#\boldsymbol{B}, \qquad \bar{\boldsymbol{K}}_1 = \boldsymbol{K}_e\boldsymbol{C}\#, \qquad \bar{\boldsymbol{K}}_2 = \boldsymbol{K}_e\boldsymbol{M}$$

and

$$\boldsymbol{K}_e = \bar{\boldsymbol{K}}_1\boldsymbol{C} + \bar{\boldsymbol{K}}_2\boldsymbol{M}\# \tag{70}$$

As shown in Ref. 20, a matrix $\boldsymbol{K}_e$ solves the subspace stabilization problem if, and only if, the following conditions on the matrices $\bar{\boldsymbol{K}}_1$ and $\bar{\boldsymbol{K}}_2$ in Eqs. (69) and (70) are met:

1) The matrix $\bar{\boldsymbol{K}}_2$ is designed to make the subspace $\boldsymbol{S}$ become invariant for Eq. (69), that is, the state motion toward the subspace, measured by the coordinate vector $\boldsymbol{\xi}_1(t)$, is decoupled from the state motion on the subspace $\boldsymbol{S}$, as measured by $\boldsymbol{\xi}_2(t)$. This requires that $\bar{\boldsymbol{K}}_2$ be such that the upper-right block of the closed-loop state matrix in Eqs. (68) and (69) becomes a zero matrix. It is also required that the same $\bar{\boldsymbol{K}}_2$ be such that a satisfactory behavior of $\boldsymbol{\xi}_2(t)$ on the subspace $\boldsymbol{S}$ is obtained. The latter behavior is represented by the eigenvalues of the matrix $\boldsymbol{R} = \bar{\boldsymbol{A}}_{22} + \bar{\boldsymbol{B}}_2\bar{\boldsymbol{K}}_2$ as shown in the following expression:

$$\begin{pmatrix}\dot{\boldsymbol{\xi}}_1 \\ \hline \dot{\boldsymbol{\xi}}_2\end{pmatrix} = \left[\begin{array}{c|c} \boldsymbol{V} & \boldsymbol{0} \\ \hline \bar{\boldsymbol{A}}_{21} + \bar{\boldsymbol{B}}_2\bar{\boldsymbol{K}}_1 & \boldsymbol{R}\end{array}\right]\begin{bmatrix}\boldsymbol{\xi}_1 \\ \hline \boldsymbol{\xi}_2\end{bmatrix} \tag{71}$$

2) The matrix $\bar{\boldsymbol{K}}_1$ is designed such that the system state $\boldsymbol{x}(t)$ promptly approaches $\boldsymbol{S}$, that is, $\boldsymbol{\xi}_1(t) \to \boldsymbol{0}$, within a specified settling time. In our case, due to the very simple structure of the matrix $\boldsymbol{A}$ in Eq. (64), the application of conditions 1 and 2, and the conversion from $\bar{\boldsymbol{K}}_1$ and $\bar{\boldsymbol{K}}_2$ to $\boldsymbol{K}_e = \bar{\boldsymbol{K}}_1\boldsymbol{C} + \bar{\boldsymbol{K}}_2\boldsymbol{M}\#$ leads to the following control-law expressions for the three channels,

$$u_{e,(\cdot)} = \left[1/\varpi M_{(\cdot)}\right]\left\{-\hat{z}_{2,(\cdot)} - \varpi\hat{z}_{2,(\cdot)} - \mu\alpha_0 x_{1,(\cdot)} + (-\mu\alpha_1 - \alpha_0)x_{2,(\cdot)} + (-\mu - \alpha_1 + \varpi)x_{3,(\cdot)}\right\}, \qquad (\cdot) = q, p, r \tag{72}$$

where the first two terms of Eq. (72) compensate for the effects of the disturbance term and the next three achieve the stabilization to the subspace $\boldsymbol{S}$. For our NASA WB001 application we will choose the parameter values $\alpha_0 = 100$, $\alpha_1 = 14$, and $\mu = 100$.

Reusable Launch Vehicle Simulation Model

This study used NASA's (WB001) lifting body model[22] as representative of a generic RLV. The model consists of separate subblocks, describing US76 atmosphere, the variation of mass, inertia, and the position of the center of gravity. A constant specific impulse is used to calculate the mass variation. The aerodynamic block models aerodynamic forces and moments resulting from the angle of attack and the sideslip angle. Attitude control is provided by the coordinated deflections of the seven nozzles associated with the WB001. We assume that three of those nozzles are oriented pitchwise to provide pitch moments, two of them are oriented yawwise to provide the yaw moment, and, finally, the differential pitch deflection of the remaining two nozzles provides roll moments.

A nonoptimum ascent profile to low circular orbit was designed to use as much as possible the aerodynamic lift during the initial part of the ascent. The orbit was attained, at 150 km of altitude, with 5% of total fuel remaining. The automatic pilot tracks the pitch angle profile until the velocity reaches 20 m/s. At this point the trajectory automatic pilot is engaged. To avoid a discontinuity, the switching is progressive with a blending of the two automatic pilot laws over a 10-s interval. A front windshear disturbance d_w represented by

$$d_w = \frac{\sigma_w}{V}\exp\left[-\left(\frac{h - 12{,}000}{4000}\right)^2\right], \qquad \sigma_w = 10 \tag{73}$$

was introduced at the level of the tropopause. The windshear equation (73) produces a flight-path disturbance having peak amplitude of 1.6 deg.

The ground track automatic pilot is used as a bank-to-turn automatic pilot during the initial and midsection of the ascent trajectory. The ground track turn-to-bank automatic pilot cannot be used before the pitch angle θ becomes smaller than 80 deg and it cannot be used for altitudes greater than 35,000 m where the degraded aerodynamic lift results in insufficient control authority for lateral maneuvers. A ground track skid-to-turn mode is used during the second half of the ascent mode, with a long progressive blending transition of the two modes. A ground track correction of 2 deg is also initiated at time = 60 s.

RLV Simulation Results

The prescribed and actual flight-path angles are shown in Fig. 3. The flight-path angle and ground track tracking errors are shown in Fig. 4, with the corresponding disturbance (73). These simulation results show an 80% cancellation of the flight-path angle disturbance. The lesser performance of the ground track autopilot compared to the flight-path autopilot performance is due to a smaller control authority. The flight-path and ground track errors at the end of the ascent are 0.5×10^{-3} and 0.02 deg, respectively.

The time variations of the angle of attack and the bank angle are plotted in Fig. 5, which illustrates the relatively large variations of those angles. The angle-of-attack, sideslip, and bank angle errors are plotted in Fig. 6. These results show that the inversion errors are

small, the largest error being an angle-of-attack error of 0.04 deg. The performance of the inner loop of control attitude tracking is illustrated in Fig. 7, which shows the prescribed and actual pitching rates. The narrow maximum of 1.5×10^{-3} deg/s appearing at time 90 s corresponds to the controller's correction of the effects of the flight-path angle disturbance. The variations of the pitching, rolling, and yawing tracking errors are shown in Fig. 8, which demonstrates that tracking of the prescribed attitude rates is excellent. The variation of the pitching actuator deflections, shown in Fig. 9, illustrates the smooth behavior of the actuators using our controller.

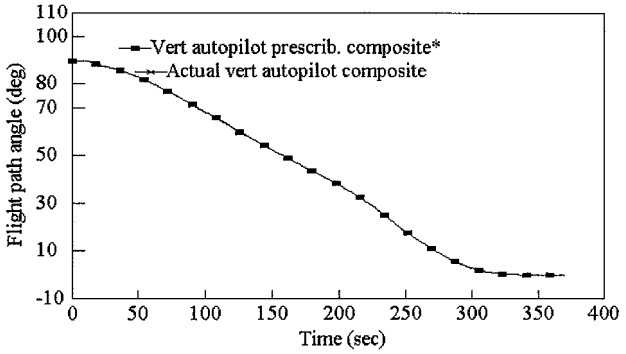

Fig. 3 Performance of flight-path automatic pilot.

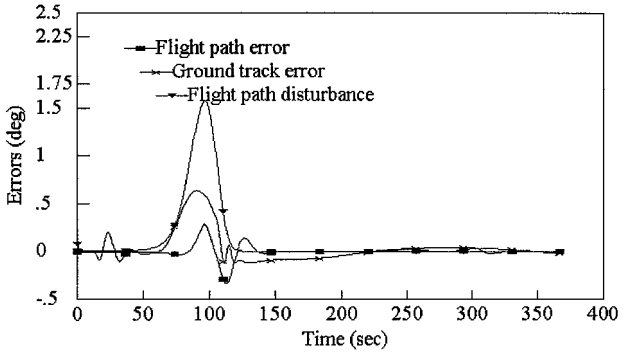

Fig. 4 Autopilot performance in the presence of a disturbance.

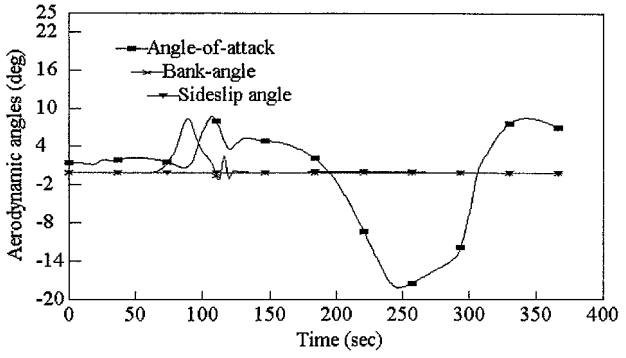

Fig. 5 Inversion: aerodynamic angles.

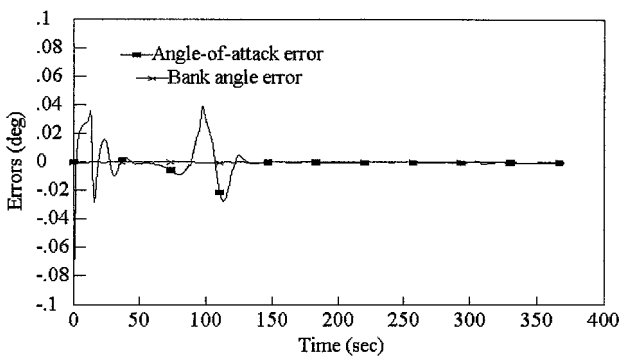

Fig. 6 Inversion errors.

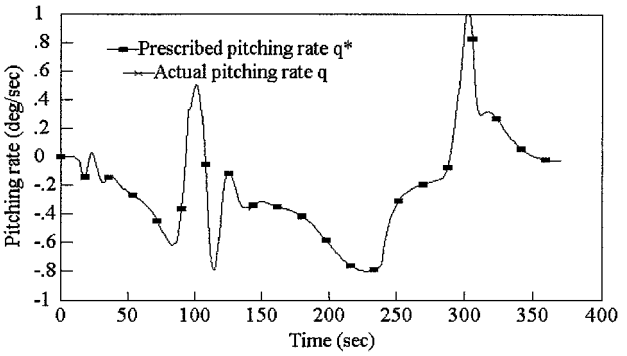

Fig. 7 Prescribed and actual pitching rates.

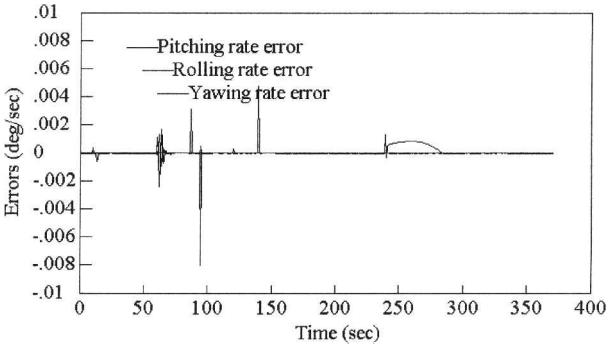

Fig. 8 Inner-loop tracking performance.

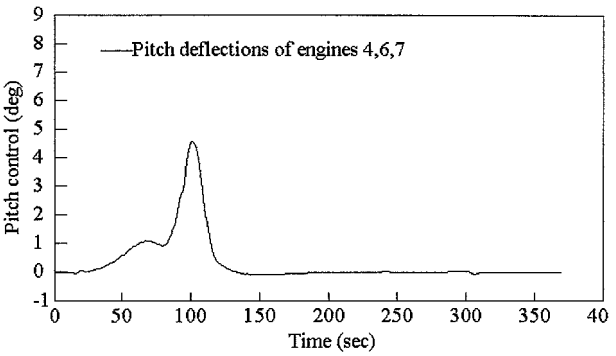

Fig. 9 Deflections of pitching actuator.

Conclusions

In this paper, a new form of flight-path angle and ground track autopilot was designed using linear-adaptive control theory. The use of DAC disturbance observers to automatically compensate for plant and disturbance uncertainties, as well as nonlinear effects, provides an effective degree of robustness in the design. The calculation of the prescribed pitch, roll, and yaw rates to be tracked in the inner loop is based on the condition $\beta = 0$. The design of the inner-loop controller is based on the technique of subspace stabilization. Its robustness is achieved through the control of the motion of tracking error to a designer-chosen performance subspace S and the use of DAC disturbance observers. The proposed design is simple and effective, as demonstrated by the simulation results obtained.

References

[1]Singh, S., and Steinberg, M., "Adaptive Control of Feedback Linearizable Nonlinear Systems with Applications to Flight Control," *Journal of Guidance, Control, and Dynamics*, Vol. 19, No. 4, 1996, pp. 871–877.

[2]Singh, S. N., Steinberg, M., and DiGirolamo, R. D., "Nonlinear Predictive Control of Feedback Linearization System and Flight Control System Design," *Journal of Guidance, Control, and Dynamics*, Vol. 18, No. 5, 1995, pp. 1023–1028.

[3]Azam, M., and Singh, S. N., "Invertibility and Trajectory Control for Nonlinear Maneuvers of Aircraft," *Journal of Guidance, Control, and Dynamics*, Vol. 17, No. 1, 1994, pp. 761–767.

[4]Gratt, H. J., and McCowan, W. L., "Feedback Linearization Autopilot Design for the Advanced Kinetic Energy Missile Boost Phase," *Journal of Guidance, Control, and Dynamics*, Vol. 18, No. 5, 1995, pp. 945–949.

[5]Adams, R. J., Buffington, J. M., Sparks, A. G., and Banda, S. S., *Robust Multivariable Flight Control*, Springer–Verlag, New York, 1994.

[6]Adams, R. J., Buffington, J. M., and Banda, S. S., "Design of Nonlinear Control Laws for High-Angle-of-Attack Flight," *Journal of Guidance, Control, and Dynamics*, Vol. 17, No. 4, 1994, pp. 737–746.

[7]Tournes, C., and Shtessel, Y. B., "Aircraft Control Using Sliding Modes Control," AIAA Paper 96-3692, 1996.

[8]Tournes, C., "Aircraft Control in Sliding Mode," M.S. Thesis, Dept. of Electrical and Computer Engineering, Univ. of Alabama in Huntsville, Huntsville, AL, Aug. 1996.

[9]Slotine, J. J., and Weiping, L., *Applied Nonlinear Control*, Prentice–Hall, Englewood Cliffs, NJ, 1991.

[10]Bugasjski, D. J., and Enns, D. F., "Nonlinear Control Law with Application to High-Angle-of-Attack Flight," *Journal of Guidance, Control, and Dynamics*, Vol. 15, No. 3, 1992, pp. 761–767.

[11]Reiner, J., Balas, G. J., and Garrard, W. L., "Robust Dynamic Inversion for Control of a Highly Maneuverable Aircraft," *Journal of Guidance, Control, and Dynamics*, Vol. 18, No. 1, 1995, pp. 18–24.

[12]Tournes, C., and Johnson, C. D., "Application of Linear Subspace Stabilization and Linear Adaptive Techniques to Aircraft Flight Control Problems: Part I the Outer-loop," *Proceedings of the Thirtieth Southeastern Symposium on System Theory*, IEEE Publications, Piscataway, NJ, 1998, pp. 150–155.

[13]Tournes, C., and Johnson, C. D., "Reusable Launch Vehicle Guidance and Control Using Subspace Stabilization Control Techniques," *Proceedings of AIAA Guidance, Navigation, and Control Conference*, AIAA, Reston, VA, 1998, pp. 183–191.

[14]Tournes, C., and Johnson, C. D., "Aircraft Guidance and Control Using Subspace Stabilization Control Techniques," *Proceedings of AIAA Guidance, Navigation, and Control Conference*, AIAA, Reston, VA, 1998, pp. 225–234.

[15]Johnson, C. D., "A Family of Linear, Time-Invariant Universal Adaptive Controllers for Linear and Nonlinear Plants," *International Journal of Control*, Vol. 49, No. 4, 1989, pp. 1217–1233.

[16]Johnson, C. D., "Example Application of the Linear Adaptive Control Technique," *International Journal of Adaptive Control and Signal Processing*, Vol. 3, 1989, pp. 111–129.

[17]Johnson, C. D., "A New Approach to Adaptive Control," *Advances in Control and Dynamic Systems*, Vol. 27, edited by C. T. Leondes, Academic, New York, 1988, Chap. 1.

[18]Johnson, C. D., "Algebraic Solution of the Servomechanism Problem with External Disturbances," *ASME Transactions, Journal of Dynamic Systems, Measurement and Control*, Vols. 96 and 97, Nos. 1 and 2, 1975, pp. 25, 161.

[19]Dorf, R. C., *Modern Control Systems*, Series in Electrical and Computer Engineering, Addison Wesley Longman, Reading, MA, 1993.

[20]Johnson, C. D., "Stabilization of Linear Dynamical Systems with Respect to Arbitrary Linear Subspaces," *Journal of Mathematical Analysis and Applications*, Vol. 44, No. 1, 1973, pp. 175–185.

[21]Johnson, C. D., "New Results in Subspace Stabilization Control Theory," *Journal of Mathematical Problems in Engineering*, Vol. 6, Nos. 2–3, 2000, pp. 99–124.

[22]Shtessel, Y. B., Tournes, C., and Krupp, D., "Reusable Launch Vehicle Trajectory Control in Sliding Modes," *Proceedings of the 1997 AIAA Guidance, Navigation, and Control Conference*, AIAA, Reston, VA, pp. 335–345.